Subantarctic Mode Water*

M. S. McCartney

Woods Hole Oceanographic Institution, Woods Hole, Massachusetts 02543, U.S.A.

Abstract—Immediately north of the circumpolar subantarctic front, deep (400–600 m) well-mixed layers are found in late winter. Spring and summer heating isolates (but does not completely erase) these layers beneath the seasonal thermocline as thermostads. The zone in which this active renewal is found is several hundred kilometers wide, but the associated thermostad can be traced much further north—on the order of 2000 km. The thermostads and the often associated dissolved oxygen maxima can be found as far north as the south equatorial current regions of each southern hemisphere subtropical gyre. This water mass formation and spreading process is equivalent to that occurring east and south of the Gulf Stream and Kuroshio currents, where the thermostads are called Subtropical Mode Water (STMW). In light of the association of these southern ocean thermostads with the circumpolar subantarctic front, rather than the subtropical fronts (western boundary currents such as the Agulhas current) the name Subantarctic Mode Water (SAMW) is suggested.

In common with STMW, SAMW contributes substantial volumetric modes to the central water masses, indicating SAMW to be the renewal agent of the high oxygen parts of the main thermocline water of the southern hemisphere subtropical gyres.

Finally, it is noted that the specific types of SAMW formed in the southeast Pacific and Scotia Sea areas are identical in temperature and salinity to the South Pacific and South Atlantic varieties of Antarctic Intermediate Water (AAIW). The renewal process for AAIW is hence indicated as taking place *north* of the polar front zone, in the southeast Pacific and Scotia Sea parts of the subantarctic zone. The actual process is late winter convective overturning of the somewhat warmer and more saline waters advecting into the region from the west along the subantarctic front. The low salinity of AAIW is due to the pronounced excess of precipitation over evaporation in the subantarctic zone. This process is quite different from the traditional concept of circumpolar cross-polar-frontal mixing of Antarctic Surface Water with Subantarctic Surface Water.

1. INTRODUCTION

DEACON's discussions of the subantarctic zone of the southern ocean (1933, 1937, 1963) have focused primarily on the origin and movement of Antarctic Intermediate Water (AAIW): the salinity minimum layer found at depths of a few hundred meters to around 1000 m in the zone, and extending off to the north at around 1000 m. AAIW is the dominant feature of the subantarctic zone in the South Atlantic Ocean, the layer there also being characterized by a dissolved oxygen maximum (DEACON, 1933; WÜST, 1935). In the remainder of the subantarctic zone, there is another feature which has not drawn as much attention as AAIW. In DEACON's (1937) review of southern ocean hydrography, the temperature distributions on Sections 9, 10 and 11 southwest and south of Australia show very thick layers at 8°–10°C lying between the Antarctic convergence and the subtropical convergence. The layers lie beneath a seasonal thermocline and are located immediately north of a pronounced thermal front (subsequently called the subantarctic

front). Seitz (1967) has coined a word for such a layer: a thermostad—a layer with a minimum vertical temperature gradient, i.e. the antonym of thermocline.

Using the much larger data collection now available from the subantarctic zone, this paper will demonstrate that the above configuration—a thermostad at intermediate depths north of the subantarctic front—is an ubiquitous feature of the subantarctic zone. This is of particular significance for our understanding of processes in the world's oceans, because identical configurations are bound in the North Atlantic and Pacific, where thermostads are found south of the Gulf Stream and Kuroshio fronts. It is interesting to find this apparent similarity of processes, since usually the zonally unobstructed southern ocean is taken to have fundamentally different physics from the zonally bounded northern hemisphere oceans.

The formation and spreading processes for the western North Atlantic thermostad has been discussed by Worthington (1959, 1972a, 1972b, 1976). He notes that a deep well-mixed layer is found in late winter immediately south and east of the Gulf Stream front. Since the thermostad is found all year round, and generally at a temperature within a few tenths of a degree of 18.0°C, he calls the layer 18° water. He also points out that an inflection point at a temperature of near 18°C exists in the temperature–depth curves well to the south of the formation site (the area where the deep well-mixed 18°C layer is found in late winter). Worthington (1972) views this southward extension of the 18° water at depths of a few hundred meters as the lower half of a meridional cell, with the surface water moving to the north, and cooling and sinking south of the Gulf Stream. Masuzawa (1969) has identified a similar layer south of the Kuroshio in the western North Pacific, at moderately cooler temperatures, and suggests the more general terminology 'Subtropical Mode Water' (STMW), subtropical referring to the formation region, and mode referring to the substantial volumetric mode this water mass contributes to each ocean's water volume. This shows up as an isolated maximum on a volumetric temperature–salinity diagram (e.g. Wright and Worthington, 1970, plate 4).

In addition to the similar thermostad/thermal front configuration, it will be demonstrated in the present paper that the formation process is identical, i.e. erosion of the seasonal thermocline during winter leaving the thermostadal layer exposed to the atmosphere in late winter, when convective overturning occurs; and that the spreading equatorward from the formation site via the subtropical gyres also is similar, although with some variation due to the circumpolar character of parts of the southern ocean circulation.

In the light of the similarity in the details of the process, the name Subantarctic Mode Water (SAMW) will be used for this thermostad. Henceforth, the abbreviations SAMW and STMW will be used.

2. THE SUBANTARCTIC MODE WATER THERMOSTAD

Three of the many meridional sections available showing the SAMW thermostad are shown in Fig. 1. Each shows a thermostadal layer extending from immediately north of a deep thermal frontal zone, well to the north through the subtropical gyres, and finally becoming indistinguishable in the south equatorial current region. Except for the associated cooler temperatures, the sections look quite similar to sections across the Gulf Stream and Kuroshio currents. The front itself is circumpolar, and will be called for simplicity the subantarctic front. The associated eastward transport can carry specific types of SAMW
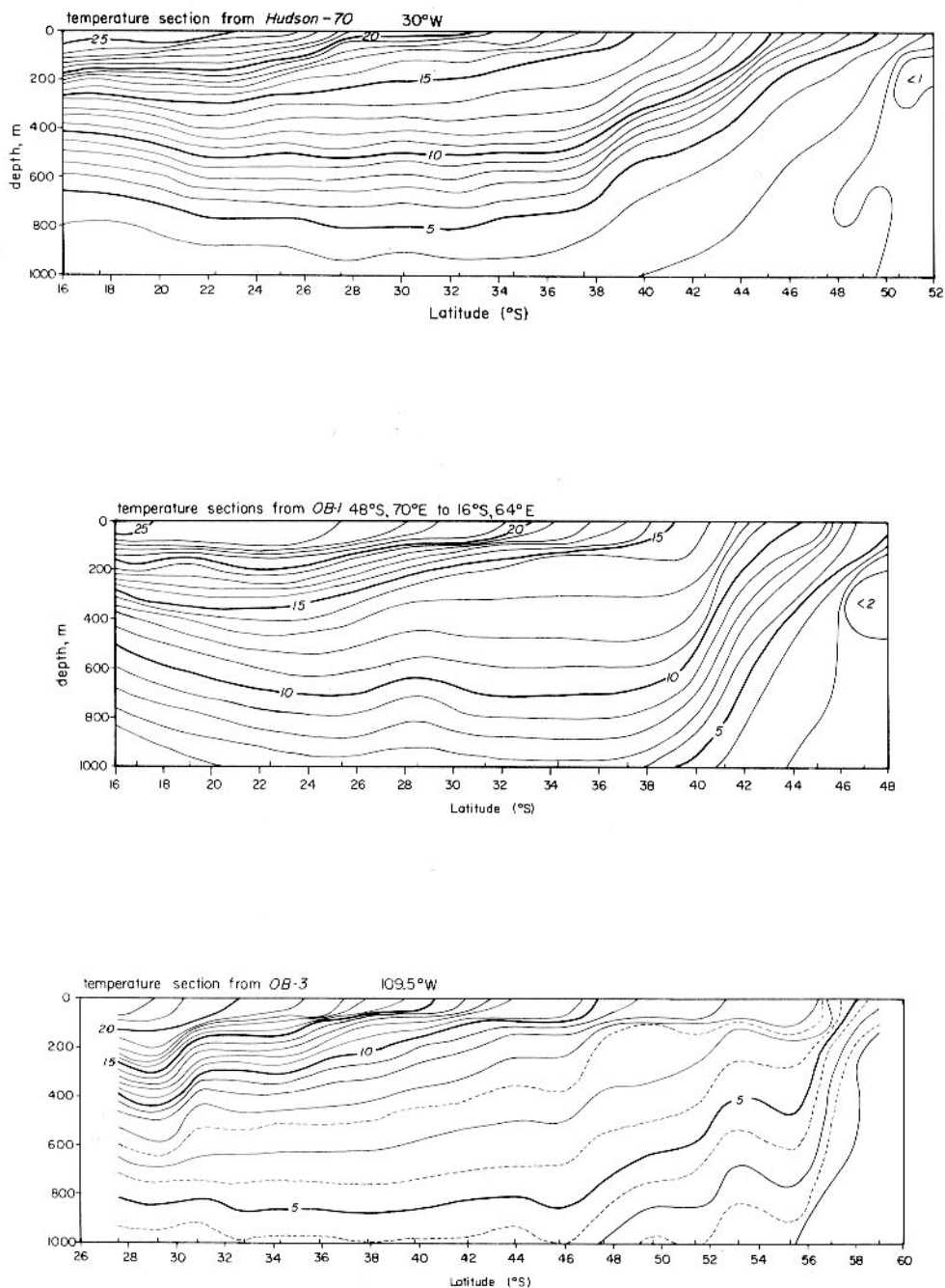
Fig. 1. Meridionally oriented temperature (°C) sections, from the Antarctic zone across the Subantarctic front, through the subtropical gyres and into the south equatorial current zone. Station latitudes are indicated by the tick marks above the latitude axis. The section locations are shown in Fig. 2. The contour interval is 1°C, except in (C), where the 3.5°, 4.5°, 5.5°, and 6.5°C isotherms are indicated by dashed lines to more clearly delineate the thermostad.

from one ocean to another, e.g. from the southeastern Pacific to the southwestern Atlantic. The 30°W section, Fig. 1a, shows the local SAMW thermostad to be centered around 14°C south of 32°S, and somewhat warmer to the north. Deacon (1937, Fig. 12) showed an expanded scale part of his earlier presented (1933) 30°W section. Station 675, at 34°S, shows a somewhat cooler thermostad—perhaps 13.5°C. This suggests a degree of climatic stability similar to 18° water (Schroeder, Stommel, Menzel and Sutcliffe, 1959).

The circumpolar character of the thermal front is indicated by the stippled thermal frontal zone on the world-chart in Fig. 2. The stippled area represents the band of high horizontal temperature gradient at 200 m on the Gordon and Goldberg (1970) atlas plate
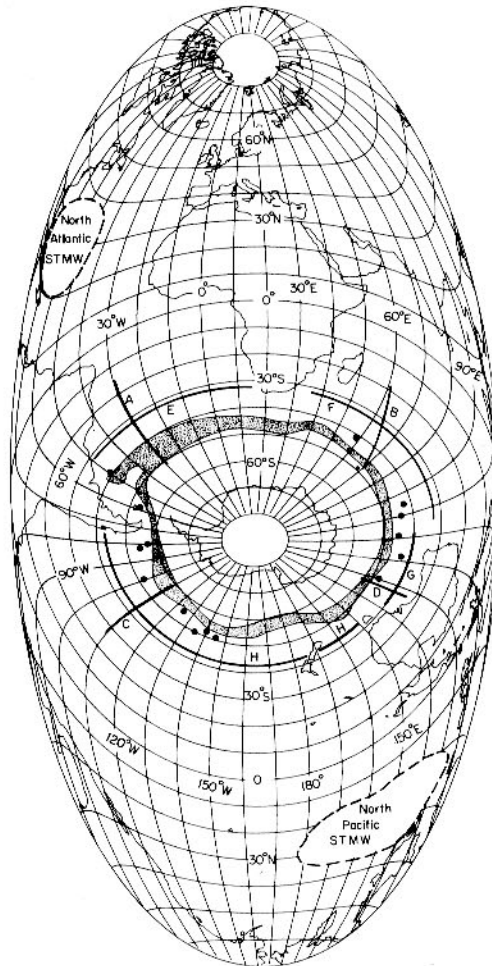

Fig. 2. World Chart: an equal-area (transversed Molleweide) projection. The subantarctic front, as determined from the high temperature gradient areas on the Gordon and Goldberg (1970) chart of temperature at 200 m, is indicated by the stippled belt between 39°S and 62°S. The regions of prevalence of STMW in the North Atlantic and North Pacific Oceans are enclosed by dashed lines. The locations of the three meridionally oriented sections presented in Fig. 1 are indicated by curves A, B and C; while that used in Fig. 6 is indicated by curve D. The four zonal sections used in constructing Fig. 4 are indicated by curves E, F, G and H. The fifteen stations used in Fig. 7 and 8 are indicated by the heavy dots.

of 200-m temperatures. This subantarctic front is spiral in nature, starting at close to 40°S in the southwestern Atlantic, and spiraling down to the east to 60°S in the southeastern Pacific. A fairly abrupt turn to the north occurs east of the Drake Passage. The temperatures associated with the front show a corresponding nearly monotonic decrease to the east from the southwestern Atlantic. There is no single indicator that can be used as front indicator, such as 15°C at 200 m is used for the Gulf Stream. Different segments of the front have been given different names in the past, with subtropical convergence being generally used in the Atlantic and southwestern Indian Oceans, and Australasian subantarctic front in the southeastern Indian Ocean (BURLING, 1961). In the Pacific, GORDON (1971) discusses the apparent double polar front zone, the northern boundary of which he calls the primary polar front, whose main characteristic is a pronounced north–south temperature gradient. Also shown on the chart in Fig. 2 are the locations of the three sections in Fig. 1, other stations and sections which will be used to further define SAMW characteristics, and for comparison to SAMW, the regions of prevalence of STMW as indicated by WORTHINGTON (personal communication) and MASUZAWA (1969). Note that the chart in Fig. 2 is an equal area projection (transversed Molleweide).

Since the GORDON and GOLDBERG (1970) atlas only covers the area south of 40°S, it misses most of the western boundary currents. The interaction between the (southward
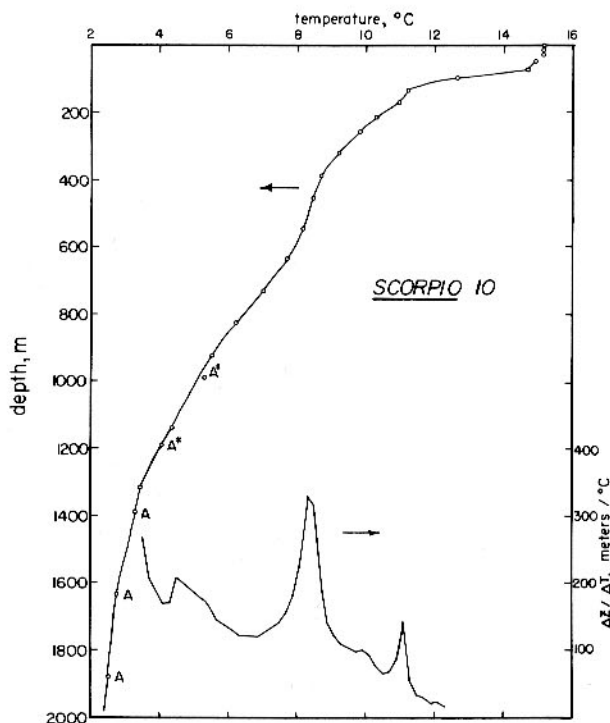

Fig. 3. Example of the three-point Lagrangian interpolated fit to Nansen bottle station data, and the resultant thermostad calculation. The station is number 10 of the SCORPIO expedition (*Eltanin* 28) and was located at 43.2°S, 161.1°E, in the Tasman Sea. The interpolated curve shown does not include the two bottles (labeled A*) from the deep cast (the remaining A bottles) which overlapped in depth the shallow cast (the unlabeled circles). The resulting $\Delta Z/\Delta T$ curve shows a possible weak near surface mode 11.1°, and the strong SAMW thermostad at 8.3°, with strength of well over 300 m/°C.

flowing) Brazil Current and the (northward flowing) Falkland Current in the southwest Atlantic is only partially resolved. This confluence extends off to the east (South Atlantic Current) accounting for the extreme breadth of the thermal frontal zone along 30°W in Fig. 1a. The Agulhas and Agulhas Return Currents lie north of 40°S, 20°E (Duncan, 1970) and account for the southward dip of the thermal frontal zone in Fig. 2 between 10° and 40°E. Two other frontal zones are not shown: the Tasman Current, extending eastward across the Tasman Sea, north of 43°S; and the confluence east of New Zealand along the Chatham Rise (43°S) between the (northeast flowing) Southland Current and the (southward flowing) East Cape Current.

To obtain a more quantitative picture of the geographical variation of thermostad strength and temperature, the following scheme was adopted: for a given hydrographic station a representation of the temperature–depth variation was obtained by using a modified Lagrangian three-point interpolation between observed data points. The resulting curve was finite-differenced to obtain estimates of inverse temperature gradient ($\Delta Z/\Delta T$) as a function of temperature, using $\Delta T = 0.2°C$. Thermostads then stand out as a maximum $\Delta Z/\Delta T$, while thermoclines are a minimum. Figure 3 shows an example of the temperature–depth fit, and the resultant $\Delta Z/\Delta T$ curve. The complete station was made up of a shallow and a deep (labeled A) cast. The deep cast had two bottles (labeled A*) which overlapped in depth with the shallow cast. A fit including these overlapping bottles would be a poor one, having an artificial inflection point in the $T–Z$ curve at 5.4°C. The station falls near the Tasman Current, and 3 hours elapsed between the messengers for the two casts; hence, ship drift in the moderately variable field of the region probably accounts for the differences between the two casts. The fit without the A* bottles looks better, although there is still a weak inflection at the join between the two casts ($T = 3.4°C$). Throughout the thermostad calculations, overlapping bottles in the deep cast were not used, and also one bottle at the join point, if the spacing at the join was less than 50 m.

Figure 4 shows the results of this thermostad calculation for a set of stations taken from four zonal sections, shown on the chart in Fig. 2: 32°S in the Atlantic Ocean (*Atlantis* cruise 247, data obtained from A. R. Miller), 32°S in the Indian Ocean (*Atlantis II* cruise 15, data obtained from NODC), 40°S in the southeast Indian Ocean (*Diamantina* cruise 1/60, data obtained from NODC), and 43°S in the Pacific Ocean (SCORPIO expedition, *Eltanin* cruise 28, data obtained from NODC). A subset of these stations spaced at nominally 5° longitude was used. The results are presented as contours of constant $\Delta Z/\Delta T = 50, 75, 100, 200$ and $300 \, m/°C$ on a temperature versus longitude diagram. It should be noted that these zonal sections lie well to the north of the formation location for SAMW (immediately north of the frontal band), so that the thermostads shown are isolated from the sea surface; that is, the local winter overturning does not extend to the depths where the thermostads are found.

The SAMW thermostad shows up as a pronounced ridge running diagonally across the diagram above the main thermocline valley. The thermostad strength is weakest in the South Atlantic, with maximum strength of about 130 m/°C near 37°W longitude (compare to the 30°W section, Fig. 2a). The thermostad temperature drops progressively to the east from the South Atlantic, while the thermostad strength increases, albeit irregularly. At 65°E the thermostad temperature is 12.7°C (compare to Fig. 2b). South of Australia and the Tasman Sea there is a leveling off of the thermostad temperature at 8–9°C. Again, climatic stability is suggested since Deacon's (1937, plates XIX and XII) sections 10 and 11 from 1932 south of Australia also show 8–9°C thermostads. On the eastern side of New

Zealand, the Chatham Rise is quite shallow, so no data at temperatures colder than 7° or 8°C is found there. East of the Rise, the SAMW thermostad reappears at 7°C, more than a full degree colder than it was west of New Zealand. Finally, just to the west of South America, the thermostad temperature has fallen to 5–6°C, with a maximum calculated thermostad strength of 447 m/°C at temperature 5.5°C, at SCORPIO 65 (*Eltanin* cruise 28, Sta. 65, 93.4°W, 43.2°S). The apparent isolated thermostad 'bubbles' at 4° to 5° are caused by the problems at the join between upper and lower casts previously mentioned. They occur at a temperature lying between that of the deepest bottle of the shallow cast, and the shallowest bottle of the deep cast, and thus are poorly defined and probably not real.

The SAMW thermostad temperature variation of from 14.5°C at 40°W to 5.5°C at 80°W averages out to an east–west temperature gradient on the order 1°C/3000 km. This is the same order of magnitude as STMW, so they have comparable longitudinal variability. STMW appears superficially more homogeneous only because of the relatively small zonal extent of its formation sites, and because it is recirculated in rather small gyres.
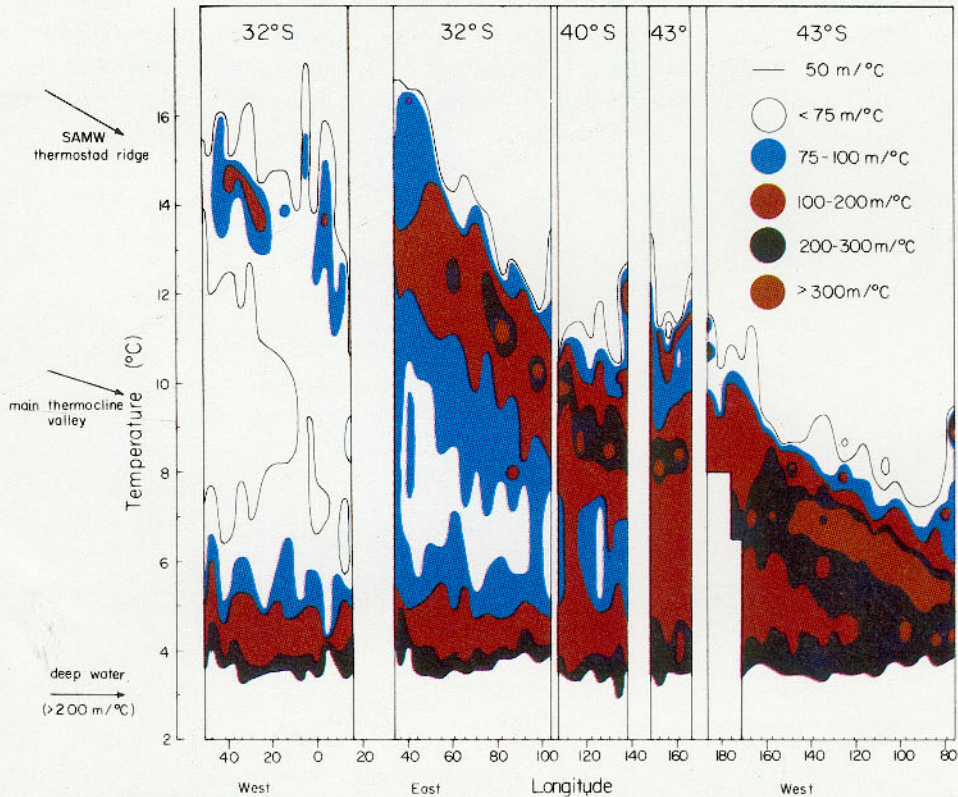

Fig. 4. Plot of the calculated thermostad strength as a function of temperature and longitude, using the four zonal sections whose positions are shown on the world chart in Fig. 2. The SAMW thermostad is the ridge running diagonally across the diagram from 14° to 15°C in the western Atlantic through 8–9°C south of Australia (120°E) and ending at 5° in the eastern Pacific. The main thermocline is the valley lying at temperatures below the ridge. No contours are shown below about 3.5°, in the more homogeneous deep water ($\Delta Z/\Delta T > 300$ m/°C). Also, no contours are shown for temperatures falling shallower than 100 m—in or above the seasonal thermocline.

3. THE FORMATION PROCESS FOR SUBANTARCTIC MODE
WATER

The formation process for STMW has been discussed by WORTHINGTON (1959, 1972a, 1972b, 1976) and WARREN (1972). They agree that the basic mechanism is vertical convective overturning at the end of winter: cooling at the surface in fall and winter, erasing the seasonal thermocline at the formation site (immediately south of the Gulf Stream and Kuroshio) allowing deep convection at the end of winter to depths on the order of 500 m. Spring warming then isolates the thermostad at depth by creating an overlying seasonal thermocline. Both authors thus emphasize the roles that the fundamentally asymmetric cooling and heating cycles play, i.e. cooling causing homogenization by convective overturning, while heating creates gradients. Further to the south, late winter overturning occurs, but not at cold enough temperatures to penetrate to the STMW thermostad. The authors disagree as to whether this process involves a net positive annual heat flux to the atmosphere (WORTHINGTON, 1972a) or essentially zero net heat flux (WARREN, 1972). They also disagree somewhat as to the details of the recirculation of STMW within the subtropical gyres.

A similar process occurs for SAMW. Figure 5 shows temperature depth profiles from a line along 128°S, south of Australia, taken between 28 August and 6 September, 1968 (late winter). The subantarctic front axis lies near Sta. 873, as can be deduced from the
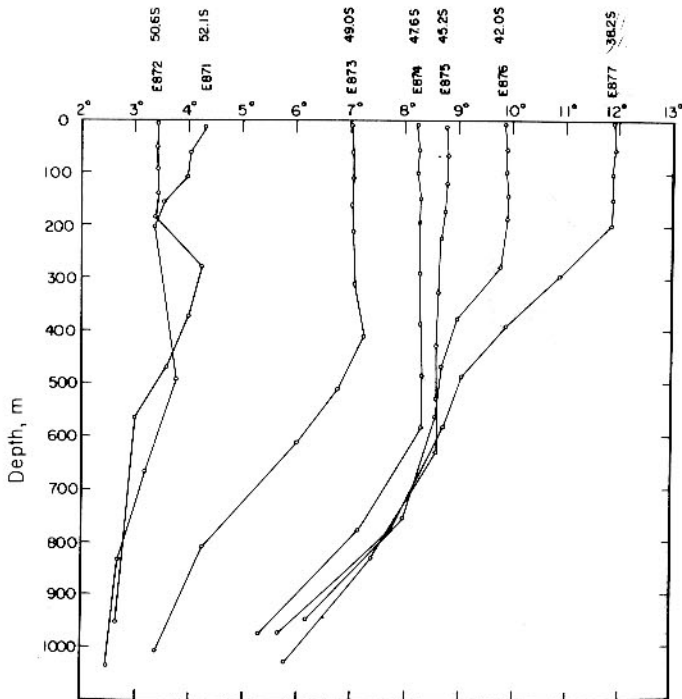

Fig. 5.   Temperature–depth profiles for a line of late-winter stations south of Australia along 128°E, taken between 28 VIII 68 and 6 IX 68, on *Eltanin* cruise 35. Stations E871 and E872 lie within the polar frontal zone, while Sta. E873 is actually within the Subantarctic front. Stations E874 and E875 show the SAMW deep mixed layer. Stations E876 and E877 have shallower, warmer mixed layers, and show the SAMW thermostad inflection point at 8–9°C.

plunging of the main thermocline between Stas. E872 and E874. The two stations north of the front (E874 and E875) show deep, well-mixed layers about 600 m in depth. Station E874 is neutrally stable for 580 m, while E875 retains a slight remnant of surface heating (only about 0.01 g/lσ_t stability). It should be noted that cooling probably lasted another month with the surface temperature reaching its seasonal minimum around the end of September. However, as WARREN (1972) has pointed out for STMW, the extreme thickness of these mixed layers precludes much change in their temperatures, even if rather extreme cooling were to persist for the entire month. The station spacing suggests a lower bound for the formation site width of $2\frac{1}{2}°$ latitude. A few 750-m XBTs were taken on this section of this cruise (*Eltanin* 35); number 49 was taken at 43.7°S, 128.0°E and showed temperature of 8.7–8.8°C over the upper 640 m. This increases the estimated formation site width to a lower bound of 3.9° latitude (430 km).

Station E873 has a 400-m mixed layer (< 0.01 g/lσ_t). This is not likely to be a volumetric mode, since it is in the middle of the front, where characteristics have a strong north–south gradient. XBTs 39 (49.3°S) and 40 (49.0°S) show temperature profiles similar to station E873, while 38 (50.2°S) has temperature less than 5°C. Thus, the width of the zone showing the station E873 mixed-layer type was greater than 0.3° latitude but probably much less than 2.6° latitude in light of the strong gradient between XBT 38 and Sta. E874.

Further north at Stas. E876 and E877 there are shallower, warmer mixed layers which do not penetrate to the depth of the 8°C thermostadal knee. These shallower mixed layers disappear almost completely in summer, as can be seen in Fig. 6. This shows a temperature section along 132°E, 4° east of the stations in Fig. 5, run in late December 1969, and January 1970 on *Eltanin* cruise 41. The section shows the SAMW in the formation zone (approximately 43° to 48°S) isolated at depth underneath a seasonal thermocline lid. Further north, the SAMW thermostad extends at a depth of 600 m all the way north to the Australian continental shelf, which lies near 34°S. It should be noted that the path of the SAMW thermostad to the Australian shelf is not along the meridional section,
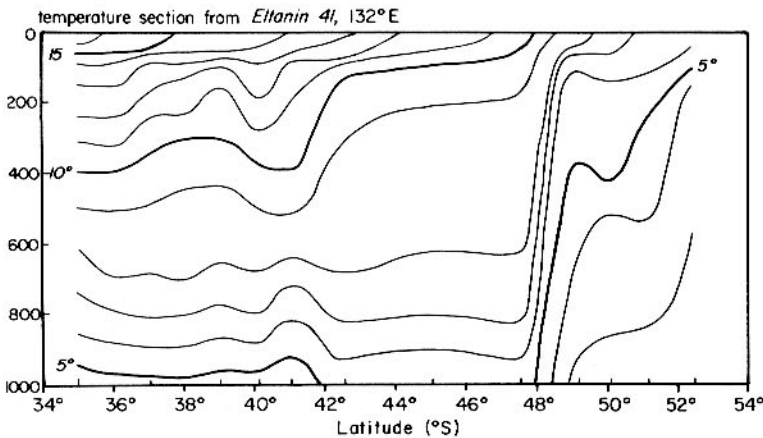
Fig. 6. A summertime temperature section south of Australia along 132°E from *Eltanin* 41. The subantarctic front is at 48° to 49°S. The SAMW north of the front is overlayed by a seasonal thermocline above 200 m, but persists as a pronounced thermostad between 200 and 600 m. North of 42°S the SAMW thermostad is still easily detectable, although not as pronounced as within the formation site between 43° and 48°S. The Australian continental shelf lies north of 35°S.

M. S. McCartney

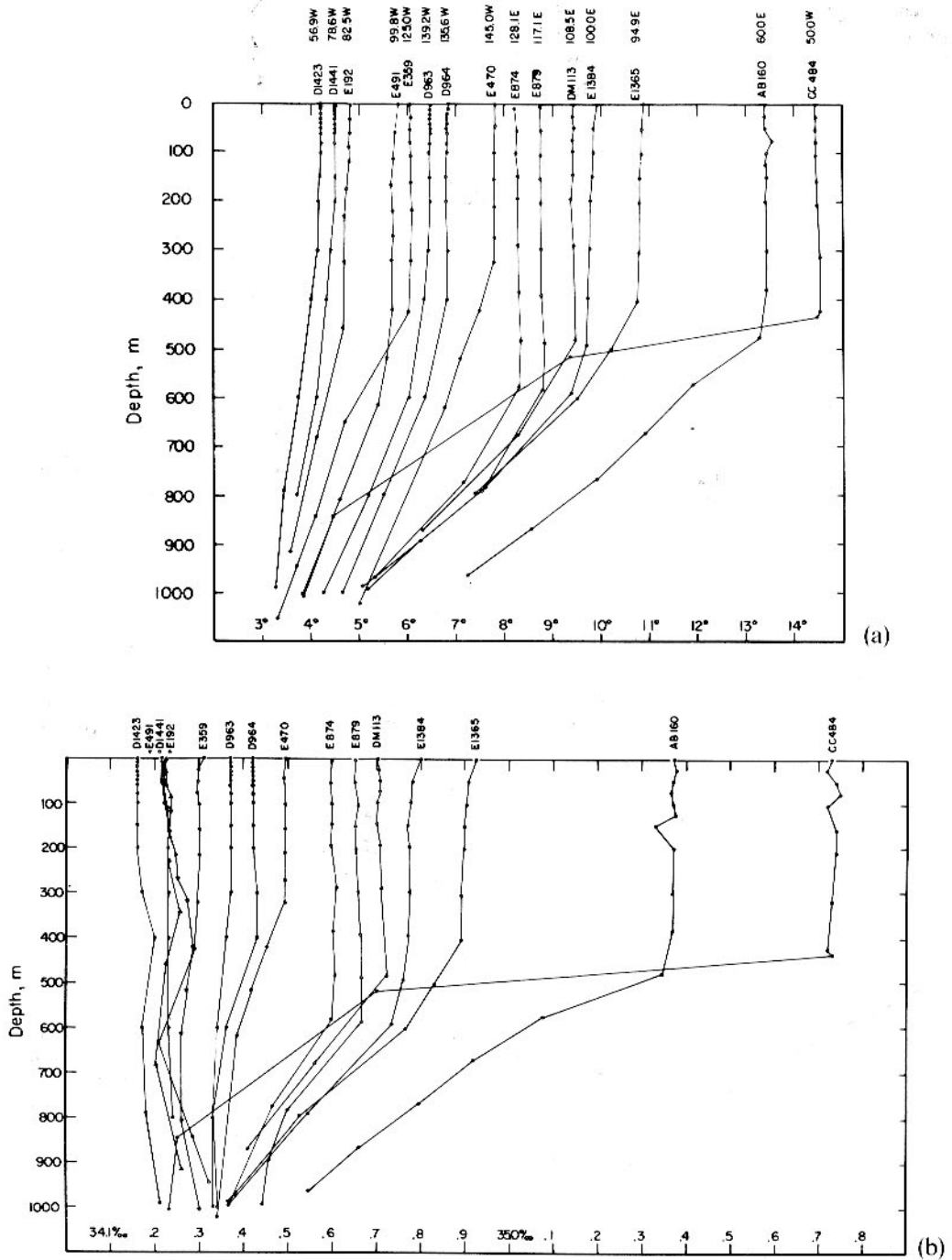Fig. 7. Temperature–depth (a) and salinity–depth (b) profiles for a group of fifteen late-winter stations from the zone immediately north of the subantarctic front. The station locations are shown on the world chart of Fig. 2; the station particulars are summarized in Table 1 in the Appendix.

but rather around the weak anticyclonic gyre within the South Australian Basin; that is, first east, then north near Tasmania, then west back to the 132° E section.

The formation zone width of a few degrees, with a formation temperature meridional variation of around $\frac{1}{2}$° C seems to be typical for the SAMW formation process circumpolarly. The longitudinal variation in characteristics within the formation zone in late winter is illustrated in Fig. 7. The figure shows temperature depth and salinity depth data for fifteen stations, whose particulars are tabulated in the Appendix; their locations are shown on Fig. 2 by the heavy dots. The stations are selected from all available cool-season extreme stations, which as far as sea surface temperature is concerned means September and October (Sta. E874 was taken on 31 August). When several stations on a given section showed the deep mixed layer, only one is shown. The fifteen stations were chosen to maximize longitudinal coverage. There are about sixteen more *Eltanin* and *Discovery* stations showing this process in the southeast Pacific, about fourteen more *Eltanin* and *Diamantina* stations in the southeast Indian Ocean, one *Anton Bruun* station in the southwest Indian and two *Capitán Cánepa* stations in the southwest Atlantic. These stations do not, however, fill any of the large longitudinal gaps in the late winter data coverage. There is a clear need for more late winter data, particularly from the southwest Pacific (southeast and southwest of New Zealand), southwest Indian (south and southeast of Madagascar, northeast and northwest of Kerguelen Island), and almost the entire South Atlantic. There is not enough data from any given region for looking in detail at year-to-year variability in formation characteristics.

The stations in Fig. 7 show mixed layers of various depths and degrees of homogeneity. The deepest and most homogeneous layers seem to be those in the southeast Indian Ocean. In general the higher the temperature of the mode, the higher the salinity; this relation making density variation rather mild (σ_t from 26.6 to 27.2, δ, from 145 to 88). The relative homogeneity of a mixed layer is probably dependent on how recently the latest deep convective event took place, and the overall intensity of the winter during that particular year. Station E470 shows a trace of thermostadal knee at 500–600 m and 6.5–7° C, suggesting that 1965 was a mild winter with overturning not penetrating all the way through the previous year's thermostad. This is further suggested by Sta. E491, from the same year, which is fairly well mixed over 300 m, but shows a high salinity layer underneath. These two stations also have rather anomalous temperature salinity relations, which will be discussed below.

Further south along the section from which Sta. D1441 was taken, the subantarctic front (GORDON's (1971) 'primary polar front') is crossed, south of which the temperature field exhibits a temperature minimum layer at around 400 m at two stations (*Discovery* Stas. 1444 and 1445). Above this layer are somewhat shallower (200–300 m) mixed layers at temperatures of 3.4–3.5° C, salinities of 34.14‰. A similar structure was observed 2 years earlier (Deacon. 1937, plate XLI). These stations were not included in Fig. 7 because they fall in the polar frontal zone rather than in the subantarctic zone. In addition, the structure may not be found every year; the stations from *Eltanin* cruise 10 along 83° W south of Sta. E192 in Fig. 7 show a single front separating the 4° subantarctic mode from the Antarctic zone, with no intervening 3° modes.

In Fig. 8, on a temperature salinity diagram, the data from the mixed layers of the fifteen stations of Fig. 7 are shown. The symbols enclose the scatter of points within the mixed layer. The 1965 anomalous Sta. E470 and E491 stand out. the former (at 7.8° C, 34.49‰) lying on the warm fresh side of the curve defined by the rest of the data, and the
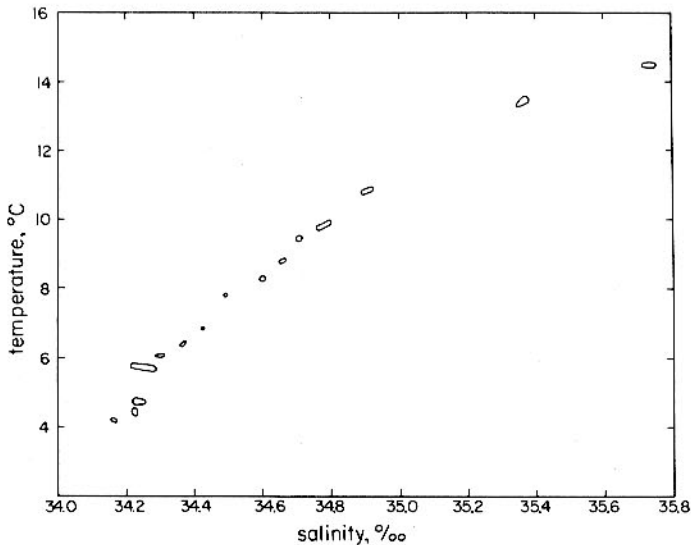
Fig. 8. Temperature–salinity diagram for the mixed layers of the stations shown in Fig. 7. The various symbols enclose the scatter of data within each of the mixed layers. The particular mixed layer depth used for each station is included in the station summary in Table 1 in the Appendix.

latter (at 5.7°C) being elongated in salinity. Stations E1365 and E1384 show compensating T–S variability, the data lines up with constant σ_t lines. The CC484 station at 14.5°C is elongated in salinity, and as a whole appears rather anomalously salty: the 14° to 15°C mode which appeared in Fig. 4 in the South Atlantic had associated salts of 35.4‰ to 35.55‰.

For comparison to Fig. 8, Fig. 9 shows the interpolated temperature–salinity data for the SAMW thermostad ridge seen in Fig. 4. The T–S arc for the 0.2° or 0.4°C range defining the maximum SAMW thermostad strength for each station has been drawn on a temperature–salinity diagram. The general agreement between the two T–S diagrams is good, except for CC484, as mentioned above.

The near linearity of groups of the data in Fig. 9 is rather remarkable. The data from the south Indian Ocean and part of the South Pacific south of the Tasman Sea (South Pacific warmer than 8°C) lies within less than 0.04‰ of the line from 8.0°C, 34.54‰ to 13.5°, 35.33‰. The data from east of the Chatham Rise (east of New Zealand) lies within 0.04‰ of the line from 5.0°C and 34.22‰ to 8.0°C and 34.51‰. The South Atlantic data seem to be divided into two groups, eastern and western, by the mid-ocean ridge at 15°W. The western group data lie within 0.02‰ of a line connecting 13.0°C, 35.25‰ and 15.0°C, 35.55‰ with the indicated thermostads having temperature between 13.2°C and 14.8°C. The eastern group data lie within 0.04‰ of a line connecting 12.0°C, 35.04‰ and 14.0°C, 35.35‰, with the indicated thermostads having temperatures between 11.2°C and 14.0°C. Thus the eastern group data are about 0.05‰ fresher than the western, in their overlapping temperature range (13°C to 14°C), and also have rather weaker thermostad strength.

The late winter data from the Pacific and Indian Oceans show a little more scatter about these lines, but this is perhaps to be expected since these data are from several
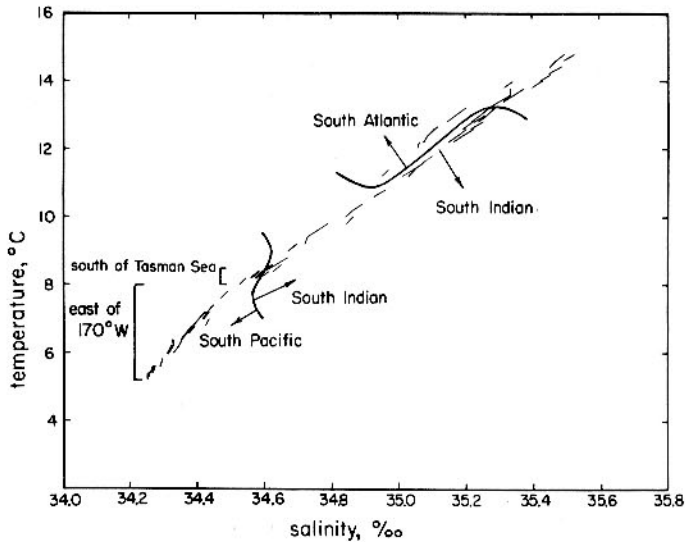
Fig. 9. Temperature–salinity diagram for the ridge defining the SAMW thermostad in Fig. 4. Each linear segment corresponds to the 0.2°C (occasionally 0.4°C) increment which has the maximum associated value of $\Delta Z/\Delta T$. The salinities were also determined by the modified three-point Lagrangian interpolation scheme.

different cruises of several different ships, with various salinity determination methods. The *Capitán Cánepa* South Atlantic station (CC484) lies 0.25‰ saltier than the western South Atlantic line. This station is rather close to the thermal front, and the high salinity may represent an effect of the southward-flowing Brazil current bringing saltier water into this area.

The isolated thermostad bubbles at 4–5°C which appeared in the South Pacific on Fig. 4 have not been included in Fig. 9, since they are probably artifacts of the calculation procedure as discussed in Section 2. Corroborating evidence for rejecting these particular indicated thermostads is that the associated data do not show the dissolved oxygen maximum which generally characterizes the SAMW thermostad. In the formation zone, the vertical overturning leads to a very high dissolved oxygen content throughout the deep mixed layer, typically 95% of saturation value or greater. North of the formation zone, the SAMW thermostads retain these high oxygen values, typically being recognizable as dissolved oxygen maximum as far north as the south equatorial current system (the northern part of the southern subtropical gyres).

4. CONCLUSIONS

The primary purpose of this paper has been to call attention to the circumpolar character of the subantarctic thermostad, the influence of the thermostad on the central water masses of the southern hemisphere oceans, and the direct analogy to processes in the northern hemisphere oceans. There have been several earlier references to local examples of specific SAMW types. DEACON (1937, p. 53) briefly mentions a 'belt of mixed water' in connection with his sections 9, 10 and 11 south and southeast of Australia. SVERDRUP,

Johnson and Fleming (1942, p. 608) used Deacon's (1937) section 10 in their discussion of Antarctic water masses. They noted the thickness of the 8–9° layer in this section south of Australia, and suggested the name Subantarctic Upper Water; although they made no further comment on it. A related observation was Wyrtki's (1962) 'Subantarctic Intermediate Water', defined as the oxygen maximum stratum found well above the Antarctic Intermediate Water salinity minimum found south of 30°S in the Tasman Sea. This seems to be the oxygen maximum associated with the 8°C SAMW in this area, so his inference that "It is likely that these values indicate water sinking in the subantarctic region" is correct.

In discussing the South Pacific sections, Deacon (1937, p. 56) gives a single sentence description of the essence of the formation process: "The observations made in the southern part of the zone in the Pacific Ocean show that in winter the water is practically uniform down to a depth of 400 m, and probably because of intense vertical mixing the surface water has almost the same properties as the subsurface and intermediate waters." Stations D963 and D964 in Fig. 7 are two of the stations on which he based this statement. In the same area of the Pacific, Mittun and Natvig (1957), using data from summer 1947 along 90°W, noted a 'quasi-homogeneous water mass' they called 'sub-Antarctic sub-surface water' lying between 100 and 400 m at a temperature of about 5.2°C.

Burling (1961) discussed the hydrography south of New Zealand, and defined two types of subantarctic water. Although not making any direct statement about the thickness, he defined an 'Australasian Subantarctic Water' at a temperature of about 8°, which is seen to be the 8–9° variety of SAMW found south of Australia (see Fig. 4). He indicates its domain to be restricted to west of the Campbell Plateau south of New Zealand, i.e. west of 170°E, agreeing with the SAMW thermostad distribution in Fig. 4. The other type, 'Circumpolar Subantarctic Water', he indicates as being colder than 8°C below the surface layer, and salinities less than 34.5‰. This would seem to be identical with the saltiest, warmest SAMW thermostads to the east of the 170°W part of Fig. 9, but this is not completely clear: the boundary between the two types is described as being the Australasian Subantarctic Front, which is simply the section of the subantarctic front south of Australia, the Tasman Sea and New Zealand. SAMW has been shown to be formed north of the subantarctic front, so there seems to be a conflict. There is very little data southeast of New Zealand that can be used to clarify the water mass and circulation picture.

There are two related items which will be pursued in later works. The first is the use of SAMW as a core layer to describe the circulation in the upper kilometer of the southern hemisphere subtropical gyres. Thermostads made perfect tracers: once isolated equatorward of the formation/renewal zone, the thermostad is a thick layer of relatively homogeneous water which, according to the meridional sections, apparently persists as it advects around the various subtropical gyres. Knowing the longitude at which a particular type (T, S) of SAMW is formed, it can be tracked around the gyre to get an indication of the upper layer circulation. A confirmation of the potential of such a calculation is the closeness of the groups of nearly linear SAMW thermostad T, S data in Fig. 9 to the linear 'central water mass' T, S curves of the subtropical southern Pacific, Atlantic and Indian Oceans, described by Sverdrup, Johnson and Fleming (1942). It is suggested that the agent of renewal of these central water masses is in fact the SAMW thermostad. Evidence for this statement is that the SAMW thermostad T, S curves in Fig. 9 overlie

the high volumetric ridges found in each of the volumetric T, S diagrams for the southern hemisphere oceans of COCHRANE (Pacific, 1958), POLLAK (Indian, 1958; more recently WYRTKI, 1971) and MONTGOMERY (Atlantic, 1958). Indeed, for the World Ocean, MONTGOMERY (1958) noted 'a strange mode' at 8.25°C, 34.65‰, which probably partially is accounted for by the rather large region of 8° SAMW south of Australia and the Tasman Sea.

The second item which would seem to warrant further study is the relation of the coldest, least saline types of SAMW to AAIW. In the southeast Pacific the deep mixed layers at the end of winter have salinities near 34.2‰ and temperatures ranging from less than 4° to about 5.5°C. These values span the range of AAIW types actually observed within the subtropical gyres. For example, JOHNSON (1972) studied the AAIW core in the South Pacific, defined as $\sigma_t = 27.10 \, \mathrm{g \cdot l^{-1}}$. On this surface he shows a tongue at salinities between 34.2‰ and 34.3‰ (temperatures of 4.5–5°C) extending north and west from the southeast Pacific subantarctic zone. The SAMW colder than 4.5° formed in the extreme southeast Pacific and Scotia Sea appears to pass through the Drake Passage and turn north past the Falkland Islands into the South Atlantic, where it forms a main contribution to the lower salinity, lower temperature variety of AAIW found in the southwest Atlantic. A major entry point of this coldest SAMW into the South Atlantic subtropical gyres seems to be the confluence region of the Brazil and Falkland currents. This can be seen in the data of Sta. CC484 in Fig. 7. At the surface is the 14°C variety of SAMW formed to the north of the confluence. At 800–1000 m is the cold (4°C), 34.2‰ variety of SAMW which has passed through the Drake Passage, turned to the north with the Falkland Current, and, being heavier, has ended up below the warmer SAMW in the confluence zone. The superposed SAMW types are separated by a very sharp pycnocline. The process of AAIW renewal just briefly described is quite different than that traditionally envisioned (e.g. SVERDRUP, JOHNSON and FLEMING, 1942, p. 619), in which AAIW formation occurs circumpolarily by cross-polar-frontal mixing of low salinity Antarctic Surface Water and Subantarctic Surface Water. The mixing product, pure AAIW, is supposed to be 2.2°C and 33.8‰ in the South Atlantic (WÜST, 1935): as it moves northward further strong, rapid mixing with the saltier waters above and below is postulated to bring the salinity up to the 34.2–34.3‰ values generally found in the subantarctic zone. In the present scheme, the renewal and recirculation of AAIW is indicated as taking place predominantly with the subantarctic and subtropical regions. The waters actually being cooled and overturned to form AAIW are just the warmer, saltier types of SAMW advecting in from the west along the subantarctic front. The low salinity of AAIW and, indeed, the entire SAMW trend of progressively lower salinities associated with the west to east trend of progressively cooler temperatures is a result of the large excess of precipitation over evaporation within the subantarctic zone, rather than injection of less saline Antarctic Surface Water across the front.

118   M. S. MCCARTNEY

REFERENCES

BURLING R. W. (1961) Hydrology of circumpolar waters south of New Zealand. *New Zealand Department of Scientific and Industrial Research Bulletin* 143, 66 pp.

COCHRANE J. D. (1958) The frequency distribution of water characteristics in the Pacific Ocean. *Deep-Sea Research*, **5**, 111–127.

DEACON G. E. R. (1933) A general account of the hydrology of the South Atlantic Ocean. *Discovery Reports*, **7**, 171–238.

DEACON G. E. R. (1937) The hydrology of the Southern Ocean. *Discovery Reports*, **15**, 1–124.

DEACON G. E. R. (1963) The Southern Ocean. In: *The Sea*, M. N. HILL, editor, pp. 281–296. Interscience, 554 pp.

DUNCAN C. P. (1970) The Agulhas Current, unpublished Ph.D. dissertation, University of Hawaii, 76 pp.

GORDON A. L. (1971) Antarctic polar front zone. In: *Antarctic Oceanology*, I, J. L. REID, editor, Antarctic Research Series, **15**, American Geophysical Union, pp. 205–221.

GORDON A. L. and R. D. GOLDBERG (1970) Circumpolar characteristics of Antarctic waters. In: *Antarctic Map Folio Series*, V. BUSHNELL, editor, American Geographical Society, **13**.

MASUZAWA J. (1969) Subtropical mode water. *Deep-Sea Research*, **16**, 463–472.

MITTUN L. and J. NATVIG (1957) Pacific Antarctic waters. *Scientific Results of the Brategg Expedition, 1947–48*, no. 3, 130 pp.

MONTGOMERY R. B. (1958) Water characteristics of Atlantic Ocean and of world ocean. *Deep-Sea Research*, **5**, 134–148.

POLLAK M. J. (1958) Frequency distribution of potential temperatures and salinities in the Indian Ocean. *Deep-Sea Research*, **5**, 128–133.

SCHROEDER E., H. STOMMEL, D. MENZEL and W. SUTCLIFFE (1959) Climatic stability of eighteen degree water at Bermuda. *Journal of Geophysical Research*, **64**(3), 363–366.

SEITZ R. C. (1967) Thermostad, the antonym of thermocline. *Journal of Marine Research*, **25**, 203.

SVERDRUP H. U., M. W. JOHNSON and R. H. FLEMING (1942) *The Oceans: their physics, chemistry and general biology*, Prentice-Hall, 1087 pp.

WARREN B. A. (1972) Insensitivity of subtropical mode water characteristics to meteorological fluctuations. *Deep-Sea Research*, **19**, 1–19.

WORTHINGTON L. V. (1959) The 18° water in the Sargasso Sea. *Deep-Sea Research*, **5**, 297–305.

WORTHINGTON L. V. (1972a) Negative oceanic heat flux as a cause of water-mass formation. *Journal of Physical Oceanography*, **2**, 205–211.

WORTHINGTON L. V. (1972b) Anticyclogenesis in the oceans as the result of outbreaks of continental polar air, 169–178. In: *Studies in Physical Oceanography*, A. L. GORDON, editor, Gordon Breach, **1**, 194 pp.

WORTHINGTON L. V. (1976) On the North Atlantic circulation. In: *The Johns Hopkins Oceanographic Studies*, R. S. ARTHUR, D. F. CARRITT, R. B. MONTGOMERY, D. W. PRITCHARD and R. O. REID, editors, The Johns Hopkins University Press **6**, 110 pp.

WRIGHT W. R. and L. V. WORTHINGTON (1970) The water masses of the North Atlantic Ocean: a volumetric census of temperature and salinity. *Serial Atlas of the Marine Environment*, W. WEBSTER, editor, folio 19.

WÜST G. (1935) Die Stratosphäre des Atlantischen Ozeans. In: *Wissenschaftliche ergebnisse der Deutschen Atlantischen Expedition auf dem Forschungs und Vermessungsschiff, Meteor 1925–1927*, Gruyter & Co., **6**(1), 109–288.

WYRTKI K. (1962) The subsurface water masses in the western South Pacific Ocean. *Australian Journal of Marine and Freshwater Research*, **13**, 18–47.

WYRTKI K. (1971) *Oceanographic Atlas of the International Indian Ocean Expedition*, National Science Foundation, 531 pp.

APPENDIX

In Table 1, the details of the fifteen late winter stations used in Fig. 7 and Fig. 8 are summarized.

Table 1.   Summary of details of the examples of late-winter hydrographic stations illustrating SAMW formation

Ship	Station	Longitude (W or E)	Latitude (°S)	Date	Depth (m)	Max. temp. (°C)	Min. temp. (°C)	Min. salin. (‰)	Max. salin. (‰)	Min. σ_t (g/l)	Max. σ_t (g/l)
								Mixed layer			
Discovery II	D1423	56.9W	53.9	25-IX-34	300	4.23	4.16	34.16	34.17	27.12	27.13
Discovery II	D1441	78.4W	55.7	26-X-34	400	4.52	4.32	34.22	34.23	27.13	27.16
Eltanin	E192	82.5W	55.1	13-X-63	458	4.83	4.61	34.224	34.256	27.10	27.13
Eltanin	E491	99.8W	52.0	23-X-65	420	5.82	5.69	34.216	34.286	26.98	27.05
Eltanin	E359	125.0W	54.9	5-IX-64	425	6.09	6.03	34.311	34.288	27.01	27.02
Discovery II	D963	139.2W	52.0	14-IX-32	400	6.48	6.34	34.37	34.36	27.02	27.02
Discovery II	D964	135.6W	49.7	15-IX-32	400	6.86	6.81	34.42	34.43	26.99	27.01
Eltanin	E470	145.0W	51.0	26-IX-65	323	7.83	7.78	34.494	34.491	26.92	26.93
Eltanin	E874	128.1E	47.6	31-VIII-68	580	8.33	8.23	34.596	34.604	26.93	26.94
Eltanin	E879	117.1E	43.0	14-IX-68	585	8.83	8.76	34.650	34.665	26.90	26.91
Diamantina	D 113	108.5E	45.3	1-X-62	484	9.48	9.38	34.699	34.724	26.83	26.85
Eltanin	E1384	100.0E	44.1	18-X-71	493	9.93	9.70	34.760	34.800	26.82	26.84
Eltanin	E1365	94.9E	42.2	29-IX-71	404	10.89	10.75	34.892	34.926	26.75	26.76
Anton Bruun	AB160	60.0E	40.9	12-IX-63	478	13.44	13.28	35.345	35.378	26.61	26.62
Capitán Cánepa	CC484	50.0W	39.4	12-IX-62	435	14.44	14.53	35.72	35.74	26.65	26.69